Available online at www.eccomasproceedia.org
Eccomas Proceedia COMPDYN (2019) 1571-1581

ECCOMAS
Proceedia

COMPDYN 2019
7th ECCOMAS Thematic Conference on
Computational Methods in Structural Dynamics and Earthquake Engineering
M. Papadrakakis, M. Fragiadakis (eds.)
Crete, Greece, 24–26 June 2019

HARNESSING TENSEGRITY TO DESIGN TUNABLE METAMATERIALS FOR BROADBAND LOW-FREQUENCY WAVE ATTENUATION

Anastasiia O. Krushynska[1], Ada Amendola[2], Raffaele Miranda[2], Chiara Daraio[3] and Fernando Fraternali[2]

[1]Engineering and Technology Institute Groningen
Faculty of Science & Engineering
University of Groningen, 9747AG, Groningen, the Netherlands
e-mail: akrushynska@gmail.com

Advanced Production Engineering,
[2] Department of Civil Engineering
University of Salerno, 84084, Fisciano (SA), Italy
e-mail: {adaamendola1, ramiranda, f.fraternali}@unisa.it

[3] Engineering and Applied Science
California Institute of Technology, Pasadena, CA 91125, USA
e-mail: daraio@caltech.edu

Abstract. *Tensegrity is a structural principle in biomechanics and architecture enabling to design rigid and mechanically stable structures by combining prestressed cables and isolated beams in compression. The present work reports a new class of tunable tensegrity-type metamaterials capable of manipulating the propagation of elastic waves by varying the level of prestrain in incorporated strings or/and manipulating the angle of rotation of inclined bars. We numerically demonstrate the generation of broadband low-frequency band gaps in the proposed meta-structures and analyze their evolution for different geometric and mechanical parameters. The transmission analysis demonstrates excellent wave attenuation efficiency by using a few metamaterial building blocks that makes the proposed meta-structures promising candidates for multiple engineering applications. Our design approach enriches the emerging class of mass-lattice metamaterials and provides meta-structures capable of attenuating elastic waves at broadband ranges in challenging low-frequency regimes.*

Keywords: Wave Dynamics, Metamaterial, Tensegrity, Band-Gap, Tunability.

ISSN:2623-3347
Peer-review under responsibility of the organizing committee of COMPDYN 2019.
doi: 10.7712/120119.7020.18419

1 INTRODUCTION

Recent progress in additive manufacturing [1, 2] has enabled the production of architected metamaterials with advanced dynamic characteristics, uncommon for natural materials. Among their properties are negative effective parameters [3], band-gap effect [3, 4, 5], acoustic cloaking [6], wave focusing [7], topologically protected states [8] (see also [9, 10, 11] for details).

Great potential for engineering applications have lattice and porous metamaterials due to their high stiffness to weight ratio and enhanced energy absorption, among others. Most such configurations have however a fixed geometry that restricts possibilities of these metamaterials for incorporating tunable functionality. Inspired by the configurational diversity of tensegrity structures, we have uncovered their potential to induce phononic band gaps at frequencies governed by the level of the structural prestress [12]. Further, we have extended the tensegrity designs to robust configurations with bending-stiff connections, less dependent on prestress, and have demonstrated strong wave suppression in light-weight meta-structures at broadband low-frequency ranges [13, 14].

As a continuation of these studies, the present work reports tensegrity-type metamaterials with mechanical and dynamic responses controlled by the rotation of the base elements. The metamaterials are composed of tensegrity prisms with solid triangular bases (Fig. 1). When prestrain in the incorporated strings is varied, the solid elements rotate relative each other, and the distance beetween them is changed. This alters the effective structural stiffness and, as a result, allows shifting the band-gap frequencies in wide frequency ranges. Through numerical simulations, we demonstrate that the rotations and involved deformations can be exploited to globally tune or even switch off the wave attenuation ability of the tensegrity-type metamaterials.

2 TENSEGRITY STRUCTURE MODEL

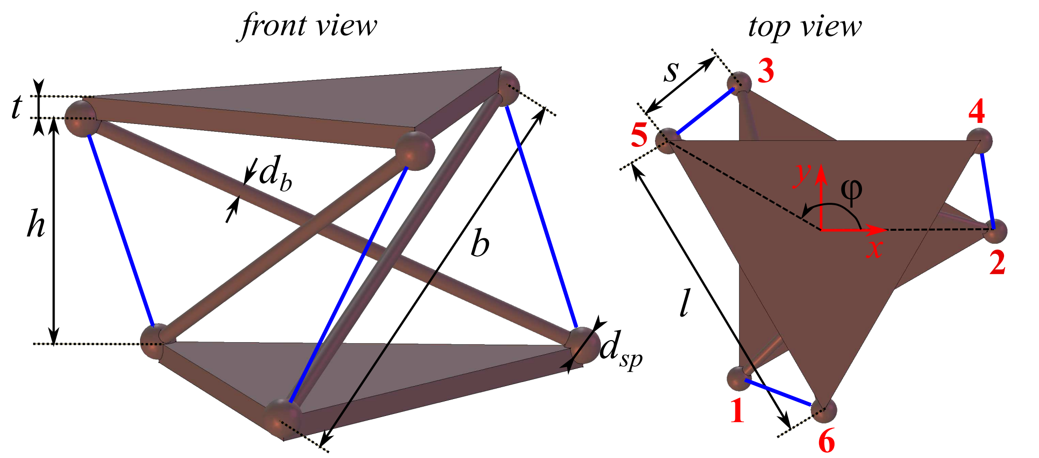

Figure 1: Configuration of a minimum regular tensegrity prism with strings indicated in blue.

We consider a three-dimensionsal tensegrity structure represented by a classic minimum regular prism (Fig. 1) [15, 16]. The two end bases, perpendicular to the central axis of the prism, are equilateral triangles of length l with vertices **1-2-3** and **4-5-6**. Three bars **1-4**, **2-5**, **3-6** and three strings **1-6**, **2-4**, **3-5** are of length b and s, respectively. For any loading, symmetric with respect to the axis of the prism, the nodal displacements of the prism can be expressed through the angle of rotation ϕ or the vertical displacement of the top base relative to the bottom.

3 STATIC ANALYSIS

We first analyze static properties of the tensegrity prism, including its stable equilibrium configuration and the axial stiffness, and establish the influence of prestress in the strings on the geometric and mechanical characteristics of the prism.

To this purpose, we assume a non-deformable, rigid behavior for the bars and the base triangles, and a linear elastic response for the strings with spring constant k_s. This assumption is reasonable for realistic structures, if the strings are more compliant than the bars [15, 16, 17]. We introduce traction-free pinned connections at the bar ends to allow free rotation of the bases.

In the Cartesian coordinates with the origin at the centroid of the bottom base, the vertices have the following coordinates: **1** $\{-a/2, -l/2, 0\}$, **2** $\{a, 0, 0\}$, **3** $\{-a/2, l/2, 0\}$, **4** $\{-l\sin(\phi)/2 - a\cos(\phi)/2, l\cos(\phi)/2 - a\sin(\phi)/2, h\}$, **5** $\{a\cos(\phi), a\sin(\phi), h\}$, and **6** $\{l\sin(\phi)/2 - a\cos(\phi)/2, -a\sin(\phi)/2 - l\cos(\phi)/2, h\}$, where $a = l/\sqrt{3}$ [17].

The constraint on a fixed length of the bars enables to estimate the height of the prism:

$$h = \sqrt{b^2 - 2a^2(1 - \cos\phi)}. \tag{1}$$

The length of the strings s is then expressed as follows:

$$s = \sqrt{b^2 + 2\sqrt{3}a^2\cos(\phi + \pi/6)}. \tag{2}$$

Let us denote the *natural* length of the string as s_N. For $s = s_N$ in the tensegrity placement, the prism can achieve a self-equilibrium condition at $\phi_0 = 5\pi/6$ under zero prestrain ($p_0 = 0$) in the strings [15]. Then, the *equilibrium* height of the prism h_0 and *equilibrium* length of the strings s_0 are

$$h_0 = \sqrt{b^2 - a^2(2 + \sqrt{3})} \qquad s_0 = \sqrt{b^2 - 2\sqrt{3}a^2}. \tag{3}$$

Since the strings are not prestrained, one obtaines $s_N = s_0$.

To mofidy the geometry of the tensegrity prism, one can apply external torque or force loading that leads to rotation of the bases relative to each other. The corresponding relations between the torque/force densities and induced vertical displacements are derived in Refs. [15, 16, 17]. Here we use another approach based on a unique feature of tensegrity designs that implies that the system can be prestressed to get the same configuration as if external loads are applied [16]. In other words, the tensegrity allows us to design various configurations by specifying an appropriate level of prestress or, equivalently, prestrain in the strings. The prestrain can be introduced, for instance, by applying external loading or using micro-stereolitography for manufacturing strings [13].

We introduce the prestrain as

$$p = \frac{s_p - s_N}{s_N}, \tag{4}$$

s_p is the length of the presstrained string. Changes is the string length induce the variation of the angle of rotation ϕ_p and the prism height h_p, which can be evaluated from (2), (1) as follows:

$$\phi_p = -\frac{\pi}{6} + \arccos\left(\frac{s_p^2 - b^2}{2\sqrt{3}a^2}\right), \qquad h_p = \sqrt{b^2 - 2a^2(1 - cos\phi_p)}. \tag{5}$$

For example, let $l = 2$ cm and $b = 2.5$ cm. Then $a = 1.15$ cm, $s_N = 1.28$ cm, and $h_0 = 1.13$ cm. The relation between the angle ϕ_p and the prestrain p is shown in Fig. 2a. As can be seen, in the absence of prestrain the prism is in self-equilibrium configuration with $\phi_p = \phi_0 = 5\pi/6$.

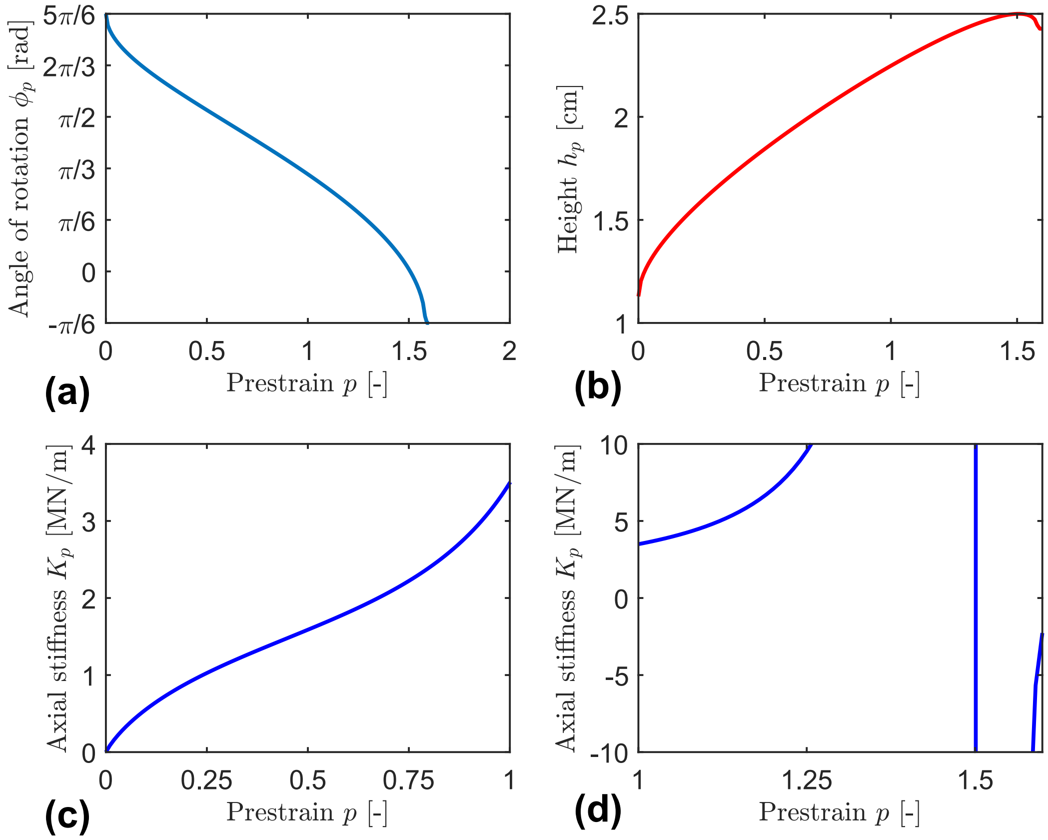

Figure 2: The relation between the prestrain in the strings and (a) the angle of rotation ϕ_p, (b) the height of the prism h_p, (c-d) the axial stiffness K_p for a minimum regular tensegrity prism with $l = 2$ cm and $b = 2.5$ cm.

As the prestrain increases, ϕ_p decreases and approaches $-\pi/6$. The increase of p above 160% leads to $(s_p^2 - b^2)/(2\sqrt{3}a^2) > 1$ in Eq. (5) that is beyond the domain of admissible arguments of function $\arccos$ for real result. (Obviously, the limiting value of the prestrain depends on l and b.) The estimated range $-\pi/6 \leq \phi_p \leq 5\pi/6$ falls within the feasible values of ϕ for a minimum regular tensegrity prism, spanning from $-\pi/3$ (the strings interfere) to π (the bars interfere) [15].

The dependence of h_p as a function of p is shown in Fig. 2b. As the prestrain increases from 0 to 1.5, the height of the prism also increases from h_0 to b corresponding to $\phi_p = 0$ when the bars are perpendicular the bases. Further increase of the prestrain naturally leads to the decrease of h_p, as the bars become inclined again.

Finally, by considering the equilibrium conditions for a prestressed prism, one can evaluate its axial stiffness (see Ref. [17] for details):

$$K_p(h_p, \phi_p) = \frac{3\sqrt{3}k_s}{\sin\phi_p}\frac{p}{1+p}\left[\sin\left(\phi_p + \frac{\pi}{6}\right) + \frac{h_p^2}{2a^2\sin^2\phi_p}\right] \quad (6)$$

$$+\frac{9k_s h_p^2}{s^2(1+p)\sin^2\phi_p}\sin^2\left(\phi_p + \frac{\pi}{6}\right), \quad (7)$$

where $k_s = E_s A_s / s_N$, E_s is the material Young's modulus, and A_s is the cross-sectional area of the spring, which is supposed to be unchanged during the deformation. One can easily see that the axial stiffness depends on the prestrain in strings and the angle of rotation ϕ_p. In the self-equilibrium state for $\phi_p = \phi_0$ and $p = 0$, K_p is zero. For very small non-zero p, we can neglect the variations of ϕ_p from ϕ_0, and the stiffness

$$K_p(h_0, \phi_0) = \frac{12\sqrt{3}k_s h_0^2}{a^2} \frac{p}{1+p} \tag{8}$$

is then governed solely by the level of prestrain. However, for larger p, the variations of ϕ_p from ϕ_0 can not be neglected. For instance, as ϕ_p approaches 0, the three terms in (7) tend to infinity. This behavior is in agreement with the introduced assumtion on infinite stiffness of the rigid bars, which appear to play the main role as ϕ_p tends to 0. Note that due to the assumption on rigid behavior of the bases and bars, their geometric parameters have no influence on the prism stiffness and can be arbitrary.

The dependence of K_p on p is illustrated in Fig. 2c,d for small/medium and large levels of the prestrain. The calculations are performed for the strings of diamater 0.28 mm made of commercially available PowerPro©Spectra fibers with Young's modulus $E_s = 5.48$ GPa [17]. The string constant is then $k_s = 0.193$ MPa·m. For different p, the prism demonstrates the nonlinear stiffening response with K_p varying in broad ranges. Hence, by varying the prestrain in the prism, one can significanlty modify its mechanical response. We use this property to design tensegrity-based metamaterials capable of attenuating elastic waves at broadband low-frequency scales.

4 TENSEGRITY-BASED METAMATERIAL

To comply with the periodicity requirements for a phononic structure, we compose a metamaterial building block from two tensegrity prisms, one of which is a mirror-reflected configuration of another along the prism axis (Fig. 3a). This ensures that for any angle of rotation ϕ_p the top and bottom bases of the building block remain parallel to each other and preserve identical coordinates in horizontal planes.

Further, we get rid of the assumption on rigid behavior of the bars and the bases and assign to them a linear elastic behavior. In this case, the static properties derived above remain valid, if the material of the bars and the bases is at least one orders stiffer than that of the strings. Finally, we replace the pinned connections between the bars and the bases by continuity conditions (bending-stiff connections). This is done, first, to simplify the envisioned experimental tests on samples manufactured by means of EBM technique, which does not allow the introduction of spherical hinges [18]. Second, as we show below, the continuity conditions allow the design of configurations with various ϕ_p, eliminating the necessity of prestrain in the strings. Note that for bending-stiff connections, the results of the conducted static analysis are unvalid, and another model, e.g. the "stick-and-spring" model, can be used to extimate the axial stiffness [18].

The dynamic analysis is performed numerically by means of the finite-element method implemented in Comsol Multiphysics 5.2. In the simulations, the bars and the bases are made of titanium alloy Ti6A14V with Young's modulus $E_t = 120$ GPa, Poisson's ratio $\nu_t = 0.33$, and mass density $\rho_t = 4450$ kg/m^3 [13], which is more than 20 times stiffer than the string material. The titanium alloy is the most widely used material in 3D-printing of metallic structures, the performance of which for manufacturing tensegrity configurations has been verified in [18]. The geometric parameters, in addition to those specified in Section 2, are the thickness of the bases $t = 1$ mm, diameter of the end spheres $d_{sp} = 1.7$ mm, and diameter of the bars $d_b = 0.7$ mm.

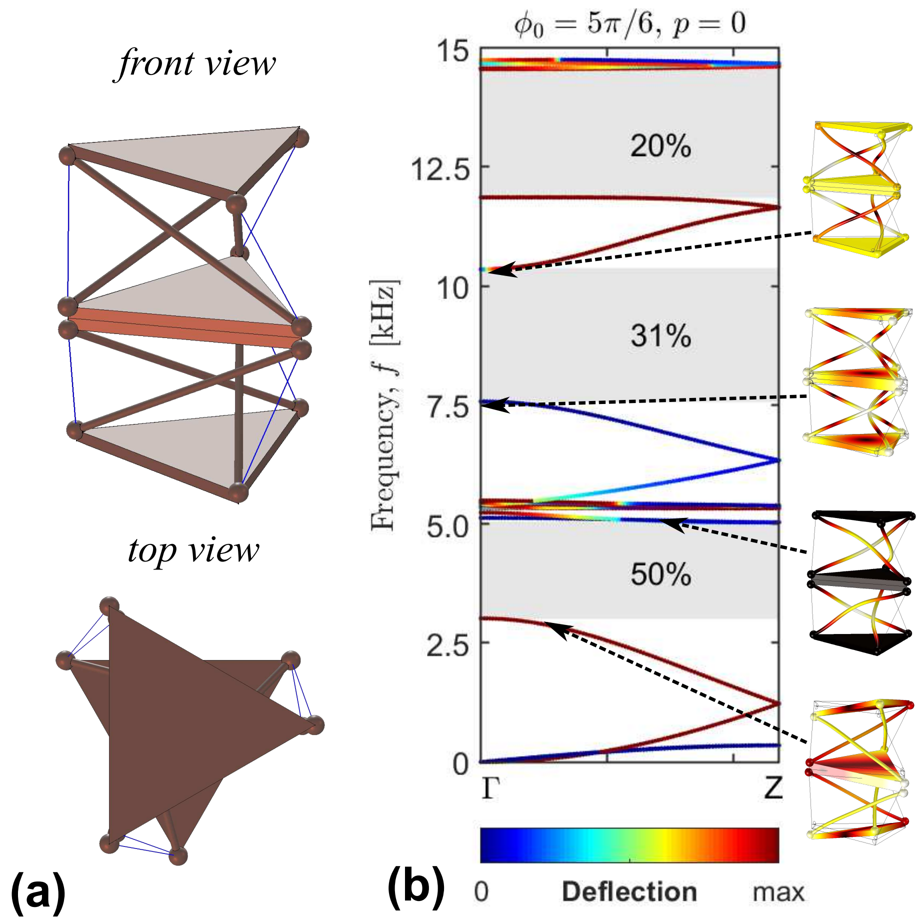

Figure 3: (a) Building block of the tensegrity-type metamaterial composed of two tensegrity prisms with one of them being the mirror-reflected of another. The top and bottom bases have identical horizontal coordinates. (b) Dispersion relation for the block with $\phi_p = \phi_0$ and zero prestrain in the strings. The insets present the mode shapes with black color indicating zero motions and bright yellow (or white) describing intense (maximum) motions.

4.1 Dispersion analysis and band-gap tunability

The wave dispersion is evaluated for a single building block with the Floquet-Bloch conditions at the external top and bottom faces. The lateral faces of the block are supposed to be free of stresses. The related eigenfrequency problem is solved for positive real wave numbers k_z varying between the edges Γ and Z of the irreducible Brillouin zone in the reciprocal space.

Figure 3b shows the dispersion relation for the tensegrity-type metamaterial with $\phi_p = \phi_0$ and $p_0 = 0$, which corresponds to the self-equilibrium state of a tensegrity prism with pinned connections. The color of the bands indicates the amount of deflection of the bases f $(0 \leq f \leq 1)$ out of the horizontal plane (the corresponding expression can be found in [13]). Specifically, almost zero values of f, indicated by blue, describe the states when movements of the bases are confined in the horizontal plane, while the values close to unity and shown by red refer to the cases with dominant motions in the axial direction. The latter type of movements is due to non-zero bending stiffness of the connections between the bases and the bars, which cannot not captured by the model developed in Section 2 [13].

The dispersion relation exhibits three low-frequency band gaps of width 50%, 31%, and 20%. Typical mode shapes are shown in Fig. 3b as insets. The mode shapes for the flat bands

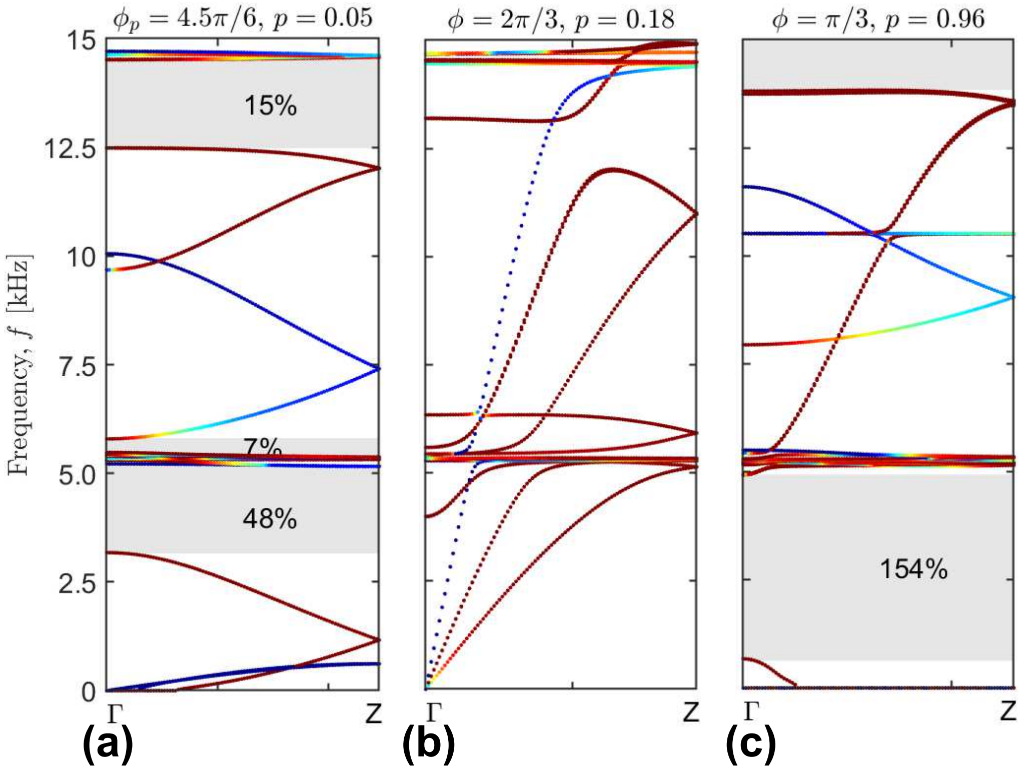

Figure 4: (a-c) Dispersion relations for the tensegrity-type metamaterial with $\phi_p = 4.5\pi/6$ (a), $\phi_p = 2\pi/2$ (b), $\phi_p = \pi/3$ (c) and the corresponding prestrain p.

describe localized resonances in the bars or the bases.

The ability of the tensegrity-type metamaterial to generate band gaps becomes even more appealing due to an additional feature of the band-gap tunability. This tunability can be understood in a global or local sense. Under the global tunability we imply the possibility to shift band gaps to different frequency ranges or wide variations of the band-gap width. The local tunability describes the cases when the band-gap bounds are up to several percent.

The local tunability is introduced by changing the prestrain in the strings. Such variations do not modify signicantly the angle ϕ_p and allow to perform fine tuning of the localized modes and the band-gap width to desired values (see Ref. [13] for more details).

The global tunability is achieved by modifying the angle of rotation ϕ_p. For example, Fig. 4a shows the dispersion relation for $\phi_p = 4.5\pi/6$. The comparison with the relation in Fig. 3 reveals that the first and the thrid band gaps are almost of the same width as those in Fig. 3b. Instead, the second gap in Fig. 4a is opened at much lower frequencies as compared to that in Fig. 3b. For $\phi_p = 2\pi/3$, all the low-frequency band gaps are closed (Fig. 4b). For $\phi_p > 2\pi/3$, the band gaps are generated again with the lower bound of the first band gap shifted to extremely low frequencies (Fig. 4c). Therefore, by changing ϕ_p, the wave attenuation performance of the the tensegrity-type metamaterial can be switch on/off or tuned to specified frequencies in a broad frequency range. It is important to remember, however, that the continuity conditions apply contraints on the variation of ϕ_p, the value of which should be specified at the manufacturing stage. At the same time, these conditions enable to eliminate prestrain in the strings that greatly simplifies the utilization of the tensegrity-type metamaterials. The underlying reason of insensitivity of the dispersion relations to p is that in the analyzed elastic model, the axial stiffness is governed by the elastic response of the bars and the bases, while the stiffness of the strings is one order lower and can be neglected. Note that the on-cite global tunability can be introduced for tensegrity structures with pinned connections that will be studied experimentally in our subsequent work.

In contrast to the most other phononic materials [19, 20, 21, 22, 23], for which the tunability requires significant modifications of the structural geometry and/or the use of specific (compliant, piezoelectric) materials, the proposed tensegrity-type metamaterials preserve their configuration. This can be explained by the presence of a specific wave attenuation mechanism relying on inertial amplification [24, 25] in addition to Bragg's scattering in thin bars and local resonances of isolated masses [13]. The comlicated interplay between various wave attenuation mechanisms induced by the peculiar geometry of the tensegrity prism allows opening extremely wide band gaps in light-weight structures (see e.g. the lowest band gap of 154% width in Fig. 4c).

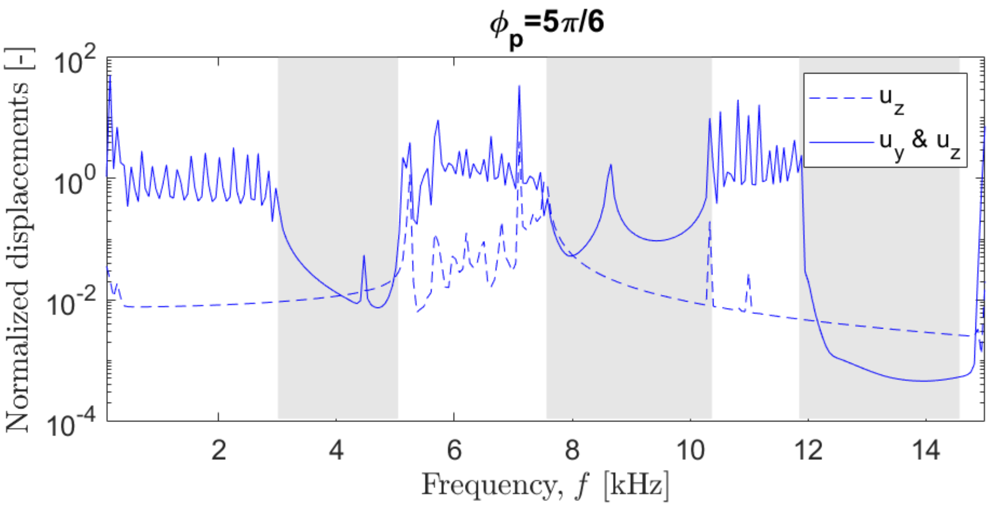

Figure 5: Normalized transmitted total displacements for a tensegrity-type metamaterial chain with $\phi_p = 5\pi/6$ averaged upon the volume of two bases of the 6th element. The shaded regions correspond to the band-gap frequencies indicated in Fig. 3b.

4.2 Transmission analysis

Finally, we estimate the wave attenuation ability of the designed metamaterials by analyzing transmission of elastic waves through a finite-size meta-chains. We consider a chain composed of 10 identical building blocks with the angle of rotation $\phi_p = 5\pi/6$, the dispersion relation of which is given in Fig. 3b.

The transmission simulations are performed in the frequency domain by using Comsol Multiphysics 5.2. One end of the sample is excited with distributed displacements u_z or u_y and u_z of magnitude 0.1 μm uniformly distributed at the triangular surface [13, 26]. The other end is attached to a perfectly matched layer (of 5 unit cell size) to minimize undesired wave reflections.

The simulation results are shown in Fig. 5 for $p = 0$ by averaging the total displacements of the bases of the 6th building block and normalizing them with respect to the applied excitation. As can be seen, in case of the axial, symmetrically distributed loading, the chain efficiently attenuates waves in very broad frequency ranges, exceeding those predicted by the dispersion analysis (the dashed blue line). It occurs since this type of loading minimizes the excitation of deflection-dominanted modes. Instead, when the non-axial loading is present (the case $u_y\&u_z$), one observes the transmission dips within the estimated band gaps, as expected. The attenuation level reaches at least 1.5 order, which is appropriate, but can be improved further by increasing the number of the building blocks.

Similar results are obtained for other angles ϕ_p. Namely, regardless of prestrain p, the transmission dips are observed within the band gaps, if the loading has non-axial components. In case of symmetrically distributed axial excitation, the wave attenuation is always enhanced.

5 CONCLUSIONS

- We analyzed the metamaterial configurations based on tensegrity structures and shown that they are capable of strongly attenuating elastic waves at broadband low-frequency scales by means of a few building blocks.

- The proposed structures are characterized by local and global tunability of the wave manipulation performance. The local tunability (fine tuning of the band-gap ranges) can be achieved by varying the prestrain in the incorporated strings. The global tunability, including switch on/off wave attenuation, is introduced by varying the angle of rotation ϕ_p of the bases relative to each other. For the analyzed bending-stiff connections between the bases and the bars, the angle can be specified only at the manufacturing stage, while truly tensegrity configurations admit on-site variations of ϕ_p and will be studied in future.

- The proposed tensegrity-type metamaterials have low mass and can be easy-to-manufacture by means of additive manufacturing techniques that makes them promising candidates for various applications including vibration mitigation, impact and shock wave protection, and others.

REFERENCES

[1] O. Al-Ketan, R.K. Abu Al-Rub, R. Rowshan, The effect of architecture on the mechanical properties of cellular structures based on the IWP minimal surface. *J. Mat. Res.*, **33**, 1-17, 2018.

[2] M.J. Mirzaali, A. Caracciolo, H. Pahlavani, S. Janbaz, L. Vergani, A.A. Zadpoor, Multi-material 3D printed mechanical metamaterials: Rational design of elastic properties through spatial distribution of hard and soft phases. *Appl. Phys. Lett.* **113**, 241903, 2018.

[3] Z. Liu, X. Zhang, Y. Mao, Y.Y. Zhu, Z. Yang, C.T. Chan, P. Sheng, Locally resonant sonic materials. *Science*, **289**, 1734-1736, 2000.

[4] J. V. Sánchez-Pérez, D. Caballero, R. Mártinez-Sala, C. Rubio, J. Sánchez-Dehesa, F. Meseguer, J. Llinares, F. Gálvez, Sound attenuation by a two-dimensional array of rigid cylinders. *Phys. Rev. Lett.*, **80**, 5325, 1998.

[5] A.O. Krushynska, V.G. Kouznetsova, M.G.D. Geers, Towards optimal design of locally resonant acoustic metamaterials. *J. Mech. Phys. Solids*, **71**, 179-196, 2014.

[6] D. Misseroni, D. Colquitt, A. Movchan, N. Movchan, I. Jones, Cymatics for the cloaking of flexural vibrations in a structured plate. *Sci. Rep.*, **6**, 23929, 2016.

[7] A. Spadoni, C. Daraio, Generation and control of sound bullets with a nonlinear acoustic lens. *Proc. Nat. Acad. Sci.*, **107**, 7230-7234, 2010.

[8] R. Fleury, A.B. Khanikaev, A. Alù, Floquet topological insulators for sound. *Nat. Comm.*, **7**, 11744, 2016.

[9] S.A. Cummer, J. Christensen, A. Alù, Controlling sound with acoustic metamaterials. *Nat. Rev. Mat.* **1**, 16001, 2016.

[10] K. Bertoldi, V. Vitelli, J. Christensen, M. van Hecke, Flexible mechanical metamaterials. *Nat. Rev. Mat.* **2**, 17066, 2017.

[11] T. Koschny, C. M. Soukoulis, M. Wegener, Metamaterials in microwaves, optics, mechanics, thermodynamics, and transport. *J. Optics*, **19**, 084005, 2017.

[12] A. Amendola, A.O. Krushynska, C. Daraio, N.M. Pugno, F. Fraternali, Tuning frequency band gaps of tensegrity metamaterials with local and global prestress. *Int. J. Solids Struct.*, **155**, 47–56, 2018.

[13] A.O. Krushynska, A. Amendola, F. Bosia, C. Daraio, N. M. Pugno, F. Fraternali, Accordion-like metamaterials with tunable ultra-wide low-frequency band gaps. *New J. of Phys.*, **20**, 073051, 2018.

[14] A.O. Krushynska, A. Amendola, F. Bosia, C. Daraio, N.M. Pugno, F. Fraternali, Tunable extremely wide low-frequency band gaps in accordion-like metamaterials. *Proc. 12th International Congress on Artificial Materials for Novel Wave Phenomena*, 237-239, 2018.

[15] I.J. Oppenheim, W.O. Williams, Geometric effects in an elastic tensegrity structure. *J. Elast.*, **59**, 51–65, 2000.

[16] R.E. Skelton, M.C. de Oliveira, *Tensegrity systems*. New-York, 2010.

[17] F. Fraternali, G. Carpentieri, A. Amendola, On the mechanical modeling of the extreme softening/stiffening response of axially loaded tensegrity prisms. *J. Mech. Phys. Solids*, **74**, 136-157, 2015.

[18] A. Amendola, A. Favata, A. Micheletti, On the mechanical modeling of tensegrity columns subject to impact loading. *Front. Mater.*, **5**, 22, 2018.

[19] C. Daraio, V.F. Nesterenko, E.B. Herbold, S. Jin, Tunability of solitary wave properties in one-dimensional strongly nonlinear phononic crystals. *Phys. Rev. E*, **73**, 026610, 2006.

[20] F. Casadei, T. Delpero, A. Bergamini, P. Ermanni, M. Ruzzene, Piezoelectric resonator arrays for tunable acoustic waveguides and metamaterials. *J. Appl. Phys.*, **112**, 064902, 2012.

[21] F. Li, D. Ngo, J. Yang, C. Daraio, Tunable phononic crystals based on cylindrical Hertzian contact. *Appl. Phys. Lett.*, **101**, 171903, 2012.

[22] P. Wang, F. Casadei, S. Shan, J.C. Weaver, K. Bertoldi, Harnessing buckling to design tunable locally resonant acoustic metamaterials. *Phys. Rev. Lett.*, **113**, 014301, 2014.

[23] V. Slesarenko, S. Rudykh, Harnessing viscoelasticity and instabilities for tuning wavy patterns in soft layered composites. *Soft Matter*, **12**, 3677-3682, 2016.

[24] C. Yilmaz, G.M. Hulbert, N. Kikuchi, Phononic band gaps induced by inertial amplification in periodic media. *Phys. Rev. B*, **76**, 054309, 2007.

[25] N. M. M. Frandsen, O.R. Bilal, J.S. Jensen, M.I. Hussein, Inertial amplification of continuous structures: large band gaps from small masses. *J. Appl. Phys.*, **119**, 124902, 2016.

[26] A.O. Krushynska, P. Galich, F. Bosia, N.M. Pugno, S. Rudykh, Hybrid metamaterials combining pentamode lattices and phononic plates. *Appl. Phys. Lett.*, **113**, 201901, 2018.